Numerical inverse scattering for the focusing and defocusing nonlinear Schrödinger equations

Thomas Trogdon[1] and Sheehan Olver[2]

[2]Department of Applied Mathematics
University of Washington
Campus Box 352420
Seattle, WA, 98195, USA

[1]School of Mathematics and Statistics
The University of Sydney
NSW 2006, Australia

May 29, 2012

Abstract

We solve the focusing and defocusing nonlinear Schrödinger (NLS) equations numerically by implementing the inverse scattering transform. The computation of the scattering data and of the NLS solution are both spectrally convergent. Initial conditions in a suitable space are treated. Using the approach of Biondini and Bui [3] we numerically solve homogeneous Robin boundary-value problems on the half line. Finally, using recent theoretical developments in the numerical approximation of Riemann–Hilbert problems, we prove that, under mild assumptions, our method of approximating solutions to the NLS equations is uniformly accurate in their domain of definition.

1 Introduction

We consider the initial-value problem on the whole line for the nonlinear Schrödinger (NLS) equation

$$\begin{aligned} iq_t + q_{xx} + 2\lambda|q|^2 q = 0, \;\; \lambda = \pm 1, \\ q(x,0) = q_0(x) \in \mathcal{S}(\mathbb{R}). \end{aligned} \tag{1.1}$$

Here $\mathcal{S}(\mathbb{R})$ denotes the Schwartz class of rapidly decaying functions. When $\lambda = 1$ we obtain the focusing NLS equation and for $\lambda = -1$, the defocusing NLS equation. The NLS equations describe physical phenomena in optics [16], Bose–Einstein condensates [12, 26], as well as water waves [29]. Together with the Korteweg-de Vries (KdV) equation, these equations are the canonical examples of the $1+1$-dimensional integrable partial differential equations.

For each of the focusing and defocusing NLS equations there exists an inverse scattering transform (IST) [30, 32]. The IST can be thought of as a nonlinear generalization of the Fourier transform on $\mathbb{R}$. The IST is, in general, equation specific in a nontrivial way. Whereas the Fourier transform solution of a linear equation will only change slightly as the dispersion relation changes, the IST changes in a much more complex way.

The presence of an oscillatory dispersive tail is seen for both the focusing and defocusing NLS equations. Small amplitude waves will travel at a speed proportional to the wave number. This dispersive tail is seen to travel in both directions. Thus, when solitons are present in the problem they may never escape the dispersion. All of these factors make traditional numerics inefficient to capture the solution for large time. The computational cost to compute the

[1]email: Sheehan.Olver@sydney.edu.au
[2]email: trogdon@amath.washington.edu

solution using time-stepping methods grows rapidly in time. The methods in [15, 11] are well suited for solving dispersive problems for small time. When a periodic approximation to the whole-line problem is used, one has to resolve the dispersive oscillations and increase the domain size as time increases. A thorough discussion of this can be found in [28] for the case of the Korteweg–de Vries (KdV) equation. In particular, it is shown that the computational costs grows at least like $t^3 \log t$.

In [28] the authors developed a numerical implementation of the inverse scattering transform (IST) for the KdV equation. The main benefit of of this method is that the computational cost to compute the solution at a given x and t value is seen to be bounded. In [28] this claim was verified with numerical tests. In [24] the authors derived sufficient conditions for bounded computational cost.

In this paper we evaluate the IST associated with the focusing and defocusing NLS equations numerically. In addition, we use symmetries to solve specific boundary-value problems on $\mathbb{R}^+$. To our knowledge this is the first time the solution of a boundary-value problem has been computed through the IST. We compute unbounded solutions to the defocusing NLS equation which have poles. Lastly, we prove that our approximation, under a specific assumption on the underlying numerical scheme, approximates solutions of (1.1) uniformly in the entire (x, t) plane. It should also be noted that the scattering problem (see Section 2) for the focusing NLS equation is a non-self adjoint spectral problem and more sophisticated analytical methods are needed but the numerical method outlined here is not adversely affected by this additional complication.

All methods we employ are demonstrated to converge spectrally. Other approaches to computing the scattering data [25, 4] are limited to second-order convergence. In [13] a method for reconstructing the solution of an integrable equation from its scattering data was developed. This method is based on the trapezoidal rule and thus does not achieve spectral convergence. Furthermore, we take advantage of contour deformation to retain accuracy for large x and t unlike the approach in [13].

2 Integrability and Riemann–Hilbert problems

The focusing and defocusing NLS equations are both completely integrable [2]. This means that for each equation there exist two linear systems of ordinary differential equations (ODEs) which depend on a spectral parameter k,

$$\begin{aligned} \mu_x &= L(k, q)\mu, \\ \mu_t &= M(k, q)\mu, \end{aligned}$$

such that $\mu_{tx} = \mu_{xt}$ if and only if q satisfies the given equation. We refer to this system of equations as the Lax pair or the scattering problem associated with the equation. We find Lax pairs for both the focusing and defocusing NLS equations through the modified Zakharov–Shabat scattering problem given by

$$\begin{aligned} \mu_x &= \begin{bmatrix} -ik & q \\ r & ik \end{bmatrix} \mu, \\ \mu_t &= \begin{bmatrix} A & B \\ C & D \end{bmatrix} \mu. \end{aligned} \tag{2.1}$$

Here q, r, A, B, C and D are scalar functions to be determined [2]. Choosing,

$$\begin{aligned} A &= -4ik^2 + iqr, \\ B &= 2qk + iq_x, \\ C &= -2rk + ir_x, \\ D &= -A, \end{aligned} \tag{2.2}$$

and $r = -\lambda\overline{q}$, we obtain Lax pairs for both the focusing and defocusing NLS equations.

The analyticity properties in k of the solutions of (2.1) are studied. For simplicity,we assume $q \in \mathcal{S}_\delta(\mathbb{R})$ where

$$\mathcal{S}_\delta(\mathbb{R}) = \left\{ f \in \mathcal{S}(\mathbb{R}) : \lim_{|x|\to\infty} |f| e^{\delta|x|} = 0 \right\}, \ \ \delta > 0.$$

Piecewise-smooth initial data with exponential decay can also be treated but this is beyond the scope of this paper. We define two matrix solutions of (2.1) by their corresponding asymptotic behavior:

$$\mu^-(x;k) \backsim \begin{bmatrix} e^{-ikx} & 0 \\ 0 & -e^{ikx} \end{bmatrix} \text{ as } x \to -\infty, \quad \mu^+(x;k) \backsim \begin{bmatrix} e^{-ikx} & 0 \\ 0 & e^{ikx} \end{bmatrix} \text{ as } x \to \infty. \tag{2.3}$$

Abel's formula implies that the determinants of these solutions are constant in x. Since the determinants are non-zero at $\pm\infty$ these matrix solutions define a linearly independent set which spans the solution space. There must exist a transition matrix

$$T(k) = \begin{bmatrix} a(k) & \mathcal{B}(k) \\ b(k) & \mathcal{A}(k) \end{bmatrix},$$

such that $\mu^+(x;k) = \mu^-(x;k)T(k)$. Define $\rho(k) = b(k)/a(k)$ to be the reflection coefficient. Some symmetry properties of T follow [2]:

$$a(k) = -\overline{\mathcal{A}(\bar{k})}, \tag{2.4}$$

$$b(k) = -\lambda\overline{\mathcal{B}(\bar{k})}. \tag{2.5}$$

For the focusing NLS equation ($\lambda = 1$) there may exist values $\kappa_j \notin \mathbb{R}$ and $\operatorname{Im}\kappa_j > 0$ such that

$$\mu_1^-(x;\kappa_j) = T(\kappa_j)\mu_2^+(x;\kappa_j), \;\; a(\kappa_j) = 0,$$

where the subscripts refer to columns. This implies that $\mu_1^-(x;\kappa_j)$ decays at both $\pm\infty$, exponentially. Thus, $\mu_1^-(x;\kappa_j)$ is an $L^2(\mathbb{R})$ eigenfunction of (2.1). From the symmetries (2.4) $\bar{\kappa}_j$ is also an $L^2(\mathbb{R})$ eigenvalue. For these values of k we define the norming constants

$$C_j = \frac{b(\kappa_j)}{a'(\kappa_j)}.$$

For the defocusing NLS equation ($\lambda = -1$) it is known there are no such eigenfunctions [2]. This implies there are no smooth soliton solutions with spatial decay for the defocusing NLS equation. We define the set

$$\left\{\rho(k), \{\kappa_j\}_{j=1}^n, \{C_j\}_{j=1}^n\right\}, \tag{2.6}$$

to be the scattering data, noting that the sets of eigenvalues and norming constants could be empty. We call the process of finding the scattering data *direct scattering*.

The solutions $\mu^\pm$ can be grouped and transformed in such a way that they satisfy a Riemann–Hilbert problem [2]. Loosely speaking, a Riemann–Hilbert problem (RHP) is a boundary-value problem in the complex plane:

Problem 2.1. *[18] Given an oriented contour $\Gamma \subset \mathbb{C}$ and a jump matrix $G : \Gamma \to \mathbb{C}^{2\times 2}$, find a bounded function $\Phi : \mathbb{C} \setminus \Gamma \to \mathbb{C}^{2\times 2}$ which is analytic everywhere in the complex plane except on Γ, such that*

$$\begin{aligned} &\Phi^+(k) = \Phi^-(k)G(k), \quad \text{for } k \in \Gamma, \text{ and} \\ &\Phi(\infty) = I, \end{aligned} \tag{2.7}$$

where Φ^+ denotes the limit of Φ as z approaches Γ from the left, Φ^- denotes the limit of Φ as z approaches Γ from the right, and $\Phi(\infty) = \lim_{|k|\to\infty}\Phi(z)$. We use $[G;\Gamma]$ to denote this RHP.

The RHP associated with the NLS equations is

$$\begin{aligned} \Phi^+(k) &= \Phi^-(k)\begin{bmatrix} 1+\lambda\rho(k)\overline{\rho(\bar{k})} & \lambda\overline{\rho(\bar{k})}e^{-\theta(k)} \\ \rho(k)e^{\theta(k)} & 1 \end{bmatrix}, \\ \Phi(\infty) &= I, \\ \theta(k) &= 2i(xk + 2tk^2), \end{aligned} \tag{2.8}$$

with the residue conditions (when $\lambda = 1$),

$$\mathrm{Res}\{\Phi(k), k = \kappa_j\} = \lim_{k\to\kappa_j} \Phi(k) \begin{bmatrix} 0 & 0 \\ C_j e^{\theta(\kappa_j)} & 0 \end{bmatrix},$$
$$\mathrm{Res}\{\Phi(k), k = \kappa_j\} = \lim_{k\to\kappa_j} \Phi(k) \begin{bmatrix} 0 & -\bar{C}_j e^{-\theta(\bar{\kappa}_j)} \\ 0 & 0 \end{bmatrix}.$$

Once the solution of the RHP is known the solution to the corresponding NLS equations is given by the expression

$$q(x,t) = 2i \lim_{|k|\to\infty} k\Phi(k)_{12},$$

where the subscript denotes the $(1,2)$ component of the matrix. We call the process of solving the RHP and reconstructing the solution *inverse scattering*.

We follow the same procedure as in [28] to turn the residue conditions into jump conditions. Fix $0 < \epsilon$ so that the circles $A_j^+ = \{k \in \mathbb{C} : |k - \kappa_j| = \epsilon\}$ and $A_j^- = \{k \in \mathbb{C} : |k - \bar{\kappa}_j| = \epsilon\}$ do not intersect each other or the real axis. We define $\hat{\Phi}$ by

$$\hat{\Phi}(k;x,t) = \begin{cases} \Phi(k;x,t) \begin{bmatrix} 1 & 0 \\ -C_j e^{\theta(\kappa_j)}/(k-\kappa_j) & 1 \end{bmatrix}, & \text{if } |k-\kappa_j| < \epsilon,\ j = 1,\dots,n, \\ \Phi(k;x,t) \begin{bmatrix} 1 & 0 \\ \bar{C}_j e^{-\theta(\bar{\kappa}_j)}/(k-\bar{\kappa}_j) & 1 \end{bmatrix}, & \text{if } |k-\bar{\kappa}_j| < \epsilon,\ j = 1,\dots,n, \\ \Phi(k;x,t), & \text{otherwise.} \end{cases} \tag{2.9}$$

It is straightforward to show that $\hat{\Phi}$ solves the RHP:

$$\hat{\Phi}^+(k) = \begin{cases} \hat{\Phi}^-(k)G(k), & \text{if } k \in \mathbb{R}, \\ \hat{\Phi}^-(k) \begin{bmatrix} 1 & 0 \\ -C_j e^{\theta(\kappa_j)}/(k-\kappa_j) & 1 \end{bmatrix}, & \text{if } k \in A_j^+, \\ \hat{\Phi}^-(k) \begin{bmatrix} 1 & -\bar{C}_j e^{-\theta(\bar{\kappa}_j)}/(k-\bar{\kappa}_j) \\ 0 & 1 \end{bmatrix}, & \text{if } k \in A_j^-, \end{cases}$$
$$\hat{\Phi}(\infty) = I,$$

where A_j^- (A_j^+) has clockwise(counter-clockwise) orientation.

We end this section with some final remarks on Riemann–Hilbert problems. Given an oriented contour Γ we define the Cauchy integral

$$\mathcal{C}_\Gamma u(k) = \frac{1}{2\pi i} \int_\Gamma \frac{u(s)}{s-k} ds.$$

It is well known that the operators defined by

$$\mathcal{C}_\Gamma^\pm u(k) = (\mathcal{C}_\Gamma u(k))^\pm,$$

are bounded operators from $L^2(\Gamma)$ to itself. Furthermore, these operators satisfy the identity

$$\mathcal{C}_\Gamma^+ - \mathcal{C}_\Gamma^- = I. \tag{2.10}$$

If we assume the solution to a RHP is of the form $\Phi = I + \mathcal{C}_\Gamma u$ we can substitute this into $\Phi^+ = \Phi^- G$ and use (2.10) to obtain

$$u - \mathcal{C}_\Gamma^- u \cdot (G - I) = G - I. \tag{2.11}$$

This is a singular integral equation (SIE) for u. We use $\mathcal{C}[G;\Gamma]$ to denote the operator in (2.11). This motivates the following definition.

Definition 2.1. *A RHP $[G;\Gamma]$ is said to be well-posed if $\mathcal{C}[G;\Gamma]$ is boundedly invertible on $L^2(\Gamma)$ and $G-I \in L^2(\Gamma)$.*

Hereafter, we assume all RHPs are well-posed.

3 Numerical direct scattering

We describe a procedure to compute the scattering data (2.6). This follows [28]. We look for solutions of the form (2.3) to (2.1). Define

$$\sigma_3 = \begin{bmatrix} 1 & 0 \\ 0 & -1 \end{bmatrix}, \quad Q = \begin{bmatrix} 0 & q \\ \lambda\bar{q} & 0 \end{bmatrix}, \quad \sigma_1 = \begin{bmatrix} 0 & 1 \\ 1 & 0 \end{bmatrix},$$

and two functions

$$\begin{aligned} J(k;x,t) &= \mu^-(k;x,t)\sigma_3 e^{ikx\sigma_3} - I, \\ K(k;x,t) &= \mu^+(k;x,t)e^{ikx\sigma_3} - I. \end{aligned} \tag{3.1}$$

Therefore $J \to 0$ as $x \to -\infty$ and $K \to 0$ as $x \to \infty$. Rewriting (2.3),

$$\mu_x = Q\mu - ik\sigma_3\mu, \tag{3.2}$$

and we find that K and J both solve

$$M_x - ik[M,\sigma_3] - Q\sigma_1 M = Q\sigma_1,$$

For each k, this can be solved with a Chebyshev collocation method on $(-\infty,0]$ for J and on $[0,\infty)$ for K using the appropriate boundary condition at infinity. (We conformally map the unbounded domains to the unit interval using $(1+x)/(1-x)$ and $(x-1)/(1+x)$.) If we use n collocation points, this gives two approximate solutions J_n and K_n for J and K, respectively. From J_n and K_n we obtain μ_n^- and μ_n^+, approximations of μ^- and μ^+, respectively, by inverting (3.1). Furthermore, μ_n^- and μ_n^+ share the point $x=0$ in their domain of definition. Define

$$T_n(k) = (\mu_n^-)^{-1}(0;k)\mu_n^+(0;k).$$

This is an approximation of the transition matrix, from which we extract an approximation of the reflection coefficient.

Remark 3.1. *Since $q_0(x)$ decays exponentially, we benefit from solving the ODEs on $[-L,0]$ and $[0,L]$ for L sufficiently large. In this case solving the equations on unbounded domains provides a good check to ensure L is sufficiently large. It can actually be shown that the resulting approximation after this truncation is an entire function of k [21].*

This procedure works well for k in a neighborhood of the real line. The solutions which decay at both $\pm\infty$ are all that is needed to obtain $b(k)$ when $a(k)=0$. Furthermore, from the analyticity properties of a we have [2]

$$\begin{aligned} a(k) - 1 &= \frac{1}{2\pi i}\int_{-\infty}^{\infty} \frac{a(s)-1}{s-k} ds, \\ a'(k) &= \frac{1}{2\pi i}\int_{-\infty}^{\infty} \frac{a'(s)}{s-k} ds. \end{aligned}$$

Thus knowing $a(k)$ on the real line and $b(k)$ when $a(k)=0$ allows us to compute $C_j = b(\kappa_j)/a'(\kappa_j)$. In practice we use the framework [23] that will be discussed in Section 4 to compute these Cauchy integrals. Also, $a'(k)$ can be obtained accurately using spectral differentiation by mapping the real line to the unit circle.

The remaining problem is that of computing κ_j. We consider (3.2)

$$\mu_x - Q\mu = -ik\sigma_3\mu, \tag{3.3}$$

$$\Rightarrow i\sigma_3\mu_x - i\sigma_3 Q\mu = k\mu. \tag{3.4}$$

We make the change of variables $x \mapsto \tan(s/2)$, $U(s) = \mu(\tan(s/2))$, $H(s) = Q(\tan(s/2))$ and we obtain

$$2i\cos^2(s/2)\sigma_3 U_s(s) - i\sigma_3 H(s)U(s) = kU(s).$$

We use Hill's method [6] to compute the eigenvalues of the operator

$$2i\cos^2(s/2)\sigma_3\frac{d}{ds} - i\sigma_3 H(s), \tag{3.5}$$

in the space $L^2([-\pi,\pi])$. Following the arguments in [28] and using the convergence of Hill's method, even for non-self adjoint operators [5, 14], the only eigenvalues we obtain off the real line are those associated with (3.3). This allows us to compute $\{\kappa_j\}_{j=1}^n$ with spectral accuracy. We can always test to make sure we have captured all eigenvalues by computing the IST at $t = 0$.

3.1 Numerical Results

In this section we present numerical results for direct scattering. First, we compare our method with a reflection coefficient that is known analytically. Next, we present numerically computed reflection coefficients, which we use later.

For the defocusing NLS equation ($\lambda = 1$) the authors in [27] present an explicit reflection coefficient for initial conditions of the form

$$q_0(x) = -iA\,\mathrm{sech}(x)\exp\left(-i\mu A\log\cosh(x)\right), \quad \mu, A \geq 0. \tag{3.6}$$

The components of the transition matrix take the form

$$a(k) = \frac{\Gamma(w(k))\Gamma(w(k)-w_- - w_+)}{\Gamma(w-w_+)\Gamma(w-w_-)},$$
$$b(k) = iA2^{-\frac{i\mu}{2}}\frac{\Gamma(w(k))\Gamma(1-w(k)+w_+ + w_-)}{\Gamma(w_+)\Gamma(w_-)},$$

where

$$w(k) = -ik - A\mu\frac{i}{2} + \frac{1}{2}, \;\; w_+ = -iA\left(T + \frac{\mu}{2}\right), \;\; w_- = iA\left(T - \frac{\mu}{2}\right),$$

and

$$T = \sqrt{\frac{\mu^2}{4} - 1}.$$

Here Γ is the Gamma function [19].

The set $\{\kappa_j\}$ is non-empty for $0 \leq \mu < 2$. Its elements are

$$\kappa_j = T - i/A(j-1/2), \; j \in \mathbb{N} \text{ and } j < 1/2 + A|T|.$$

In Figure 1 we plot the reflection coefficient for $A = 1$ and $\mu = 0.1$. These plots demonstrate spectral convergence.

In Figure 2 we show the reflection coefficient for $q_0(x) = 1.9\exp(-x^2 + ix)$ for both focusing and defocusing NLS. For focusing NLS we find $\kappa_1 = -0.5 + 1.11151i$, see Figure 2(c) for a plot of the spectrum of (3.5) found using Hill's method.

4 Numerical inverse scattering

Numerical inverse scattering has two major components. The first is the use of a Chebyshev collocation method for solving RHPs [23] and the second is the deformation of contours in the spirit of the method of nonlinear steepest descent (NSD) [7]. The use of NSD is essential since the jump for the RHP (2.8) is oscillatory for large values of x and t. An interesting and desired consequence of using NSD is that the resulting numerical method is accurate for large values of x and t. More specifically, the computational cost to compute the solution at a given point, accurate to within a given tolerance, is shown to be independent of x and t (see Section 7). First, we describe the collocation method for RHPs and then deform the RHP (2.8) to produce an efficient numerical method.

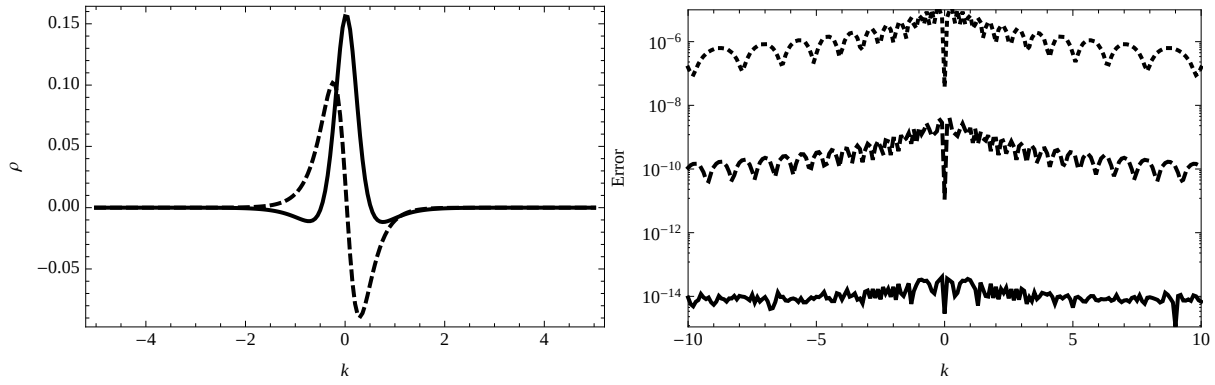

Figure 1: (a) Plot of the known analytical formula for the reflection coefficient with $A = 1$ and $\mu = 0.1$ (Solid: real part, Dashed: imaginary part). (b) Demonstration of spectral convergence for the reflection coefficient (Dotted: 40 collocation points, Dashed: 80 collocation points, Solid: 120 collocation points.).

Consider the contour $\Gamma = \bigcup_{j=1}^{n} \Gamma_j$ where each Γ_j is a non-self-intersecting arc. We use γ_0 to denote the set of self-intersections of Γ. Assume we have a sequence of Möbius transformations $M_1, \ldots, M_n$ such that $M_k([-1, 1]) = \Gamma_k$. Define $\mathbb{P}_m = \{\cos(j\pi/m) : j = 0, 1, \ldots, m\}$, the Chebyshev points, and let $T_m(x)$ denote the mth Chebyshev polynomial of the first kind. Given a RHP

$$\Phi^+(k) = \Phi^-(k)G(k), \;\; k \in \Gamma, \;\; \Phi(\infty) = I, \tag{4.1}$$

which satisfies compatibility conditions at the self-intersection points of Γ, the framework in [23] will generally return a vector W_j of values at the mapped points $M_j(\mathbb{P}_{n_j})$, so that the function $W : \Gamma \to \mathbb{C}^{2\times 2}$ defined piecewise by

$$\begin{aligned} W(k)|_{\Gamma_j} &= \sum_{i=0}^{n_j} \alpha_i T_i(M_j^{-1}(k)), \\ W(M(\mathbb{P}_{n_j})) &= W_j, \end{aligned}$$

satisfies

- $I + \mathcal{C}_\Gamma v$ is bounded, and
- $I + \mathcal{C}_\Gamma v$ satisfies the RHP (4.1) exactly at $M_j(\mathbb{P}_{n_j})$.

All RHPs considered here satisfy the conditions needed to apply the framework in [23].

We describe briefly the approach of this framework. A closed-form expression [22] for the Cauchy transform of the basis $T_i(M_j^{-1}(k))$ allows the discretization $\mathcal{C}_n[G;\Gamma]$ of (2.11) by evaluating the Cauchy transform of the basis at the points $M_j(\mathbb{P}_{n_j})$. A modified definition for the Cauchy transform is required at the junction points γ_0 (which are included in the collocation points $M_j(\mathbb{P}_{n_j})$), at which the Cauchy transform of this basis is unbounded. By assuming that the computed W is in the class of functions for which $I + \mathcal{C}_\Gamma v$ is bounded, we define the bounded contribution of the Cauchy transform of each basis element at the points γ_0. A consequence of solving the resulting linear system is that the numerically calculated W must be in this class of functions. Therefore $I + \mathcal{C}_\Gamma W$ is bounded and satisfies the RHP at γ_0, hence at all points in $M_j(\mathbb{P}_{n_j})$.

If $\Phi(\infty) = 0$ and $W \in L^1(\Gamma)$ then

$$\lim_{k\to\infty} k\Phi(k) = -\frac{1}{2\pi i}\int_\Gamma W(t)dt, \tag{4.2}$$

by dominated convergence. The integral on the right-hand side is computed using Clenshaw–Curtis quadrature. This relationship is needed in what follows to reconstruct the solution of an NLS equation from the solution of the RHP. The framework in [22, 23] gives an efficient method for computing $\mathcal{C}_\Gamma$ off Γ as well.

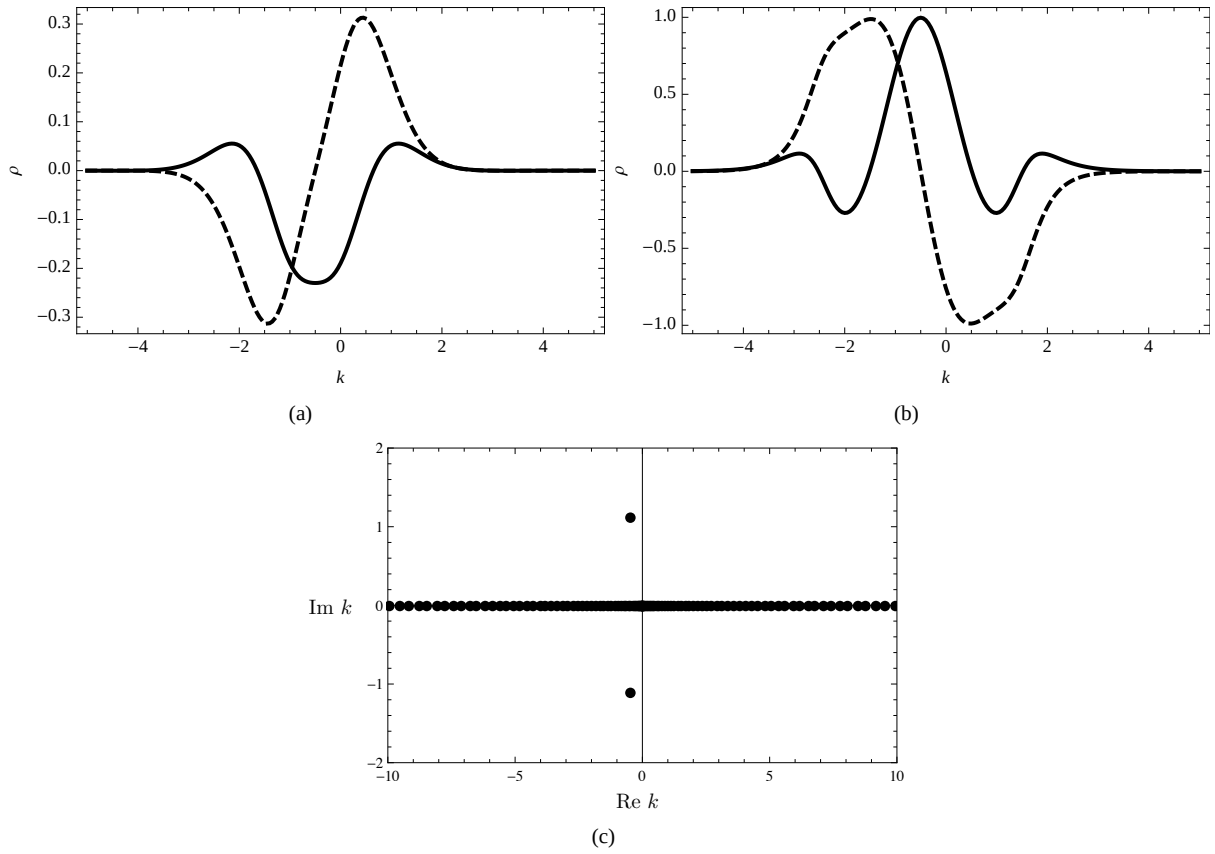

Figure 2: (a) Plot of known reflection coefficient for the focusing NLS equation ($\lambda = 1$) when $q_0(x) = 1.9e^{-x^2+ix}$. (Solid: real part, Dashed: imaginary part). (b) Plot of known reflection coefficient for the defocusing NLS equation ($\lambda = -1$) when $q_0(x) = 1.9e^{-x^2+ix}$. (Solid: real part, Dashed: imaginary part). (c) The spectrum of (3.5) found using Hill's method when $\lambda = 1$.

The spectral convergence of this method is guaranteed provided that the norm of inverse of the discretized operator $\mathcal{C}_n[G;\Gamma]$ does not grow too rapidly [23, 24]. We make the following assumption.

Assumption 4.1. *If G is continuous and $[G;\Gamma]$ is well-posed then*

$$\|\mathcal{C}_n[G;\Gamma]^{-1}\|_n \leq Cn^{\beta}\|\mathcal{C}[G;\Gamma]^{-1}\|_2, \quad \beta > 0,$$

where $\|\cdot\|_2$ is the induced operator norm on $L^2(\Gamma)$ and $\|\cdot\|_n$ is an appropriate finite-dimensional operator norm, see [24].

Remark 4.1. *As previously mentioned, the jump matrix G needs to satisfy a compatibility condition at each point in γ_0. The description of this is beyond the scope of this paper, see [24] for details.*

Furthermore, the results in [24] justify the truncation of contours when they are, to machine precision, the identity matrix. This allows us to consider all RHPs on appropriate contours of finite length.

Remark 4.2. *A* `Mathematica` *implementation of the the framework in [23] is available online [20].*

4.1 Small time

When both x and t are small, the RHP needs no deformation. When t is small, but x is large, the RHP needs to be deformed. We introduce factorizations of the jump matrix. Define

$$
\begin{aligned}
G(k) &= \begin{bmatrix} 1-\lambda\overline{\rho(\bar{k})}\rho(k) & \lambda\overline{\rho(\bar{k})}e^{-\theta(k)} \\ \rho(k)e^{\theta(k)} & 1 \end{bmatrix}, \\
M(k) &= \begin{bmatrix} 1 & \lambda\overline{\rho(\bar{k})} \\ 0 & 1 \end{bmatrix}, \qquad P(k) = \begin{bmatrix} 1 & 0 \\ \rho(k)e^{\theta(k)} & 1 \end{bmatrix}, \\
L(k) &= \begin{bmatrix} 1 & 0 \\ \frac{\rho(k)}{\tau(k)} & 1 \end{bmatrix}, \qquad D(k) = \begin{bmatrix} \tau(k) & 0 \\ 0 & 1/\tau(k) \end{bmatrix}, \qquad U(k) = \begin{bmatrix} 1 & \frac{\lambda\overline{\rho(\bar{k})}}{\tau(k)} \\ 0 & 1 \end{bmatrix}, \\
\tau(k) &= 1-\lambda\rho(k)\overline{\rho(\bar{k})}.
\end{aligned}
\tag{4.3}
$$

Note that $G(k) = L(k)D(k)U(k) = M(k)P(k)$. We assume the sets $\{\kappa_j\}_{j=1}^n$ and $\{C_j\}_{j=1}^n$ are empty. Later make the proper modifications to incorporate the extra contours required otherwise

We wish to deform contours of (2.8) off the real line so that oscillations are turned to exponential decay. The matrix G contains the two factors $\exp(\pm\theta(k))$ and if one decays the other must grow. This motivates separating these factors using the process of *lensing* [7]. Suppose we can factor the jump function as ABC. It is possible to separate the single contour into three contours, as in Figure 3, assuming A and C are analytic in a sufficiently large neighborhood of the original contour and continuous up to the new contour. If $\tilde{\Phi}$ satisfies the jumps on the split contour, it is clear that we can recover Φ by defining $\Phi = \tilde{\Phi}C$ between the top contour and the original contour, $\Phi = \tilde{\Phi}A^{-1}$ between the original contour and the bottom contour, and $\Phi = \tilde{\Phi}$ everywhere else, see the bottom of Figure 3. It is important to note that the limiting properties of Φ and $\tilde{\Phi}$ at infinity are the same.

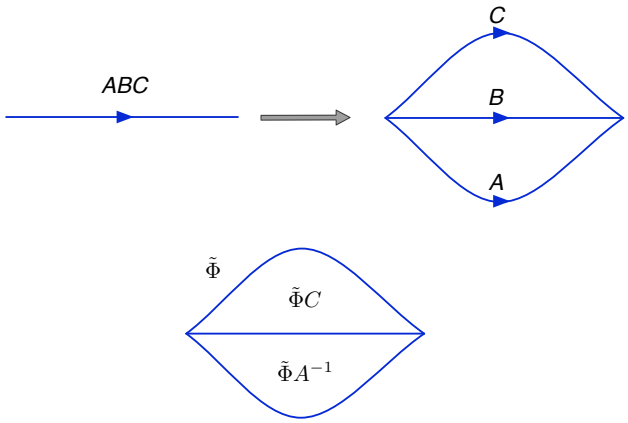

Figure 3: Demonstration of the lensing process.

Since $q_0(x) \in \mathcal{S}_\delta(\mathbb{R})$ for some $\delta > 0$ it follows that ρ is analytic in some strip $S_\gamma = \{k \in \mathbb{C} : |\operatorname{Im} k| < \gamma\}$ for $\gamma > 0$. This can be seen by considering the Volterra integral equations for the eigenfunctions $\mu^\pm$. The factors in (4.3) allow lensing but we need to determine where to lens. We look for stationary points of the oscillator: $\theta'(k) = 0$ when $k = k_0 = -x/(4t)$. We use the LDU factorization for $k < k_0$ and MP for $k > k_0$. See Figure 4(b) for this deformation and note that the contours are locally deformed in the direction of steepest descent, that is, the direction along with the jump matrix tends to the identity matrix most rapidly. We denote the solution of this lensed RHP by Φ_1.

This RHP can be solved numerically provided t is not too large. As t increases, the solution v on the contour $(-\infty, k_0)$ is increasingly oscillatory and is not well resolved using Chebyshev polynomials.

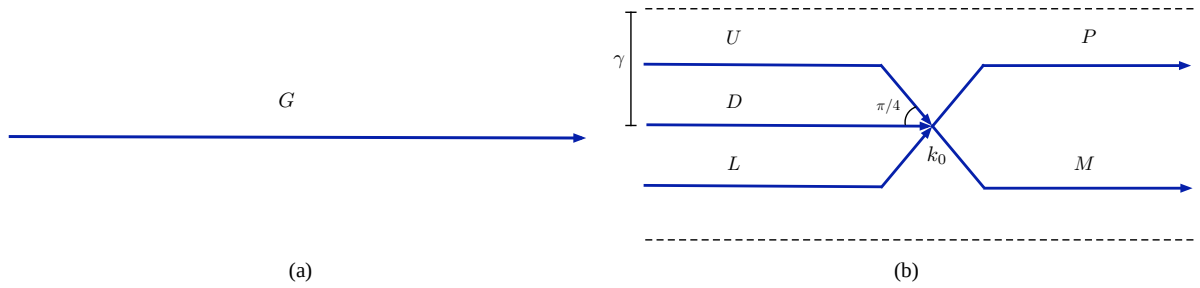

(a) (b)

Figure 4: (a) Jump contour for the initial RHP for Φ. (b) Jump contours after lensing for the RHP for Φ_1.

4.2 Long time

Next, we provide a deformation that leads to a numerical method that is accurate for arbitrarily large x and t. In light of the results in [24], we need to remove the contour D from the RHP so that all jumps decay to the identity matrix away from k_0 as x and t become large. The matrix-valued function

$$\Delta(k;k_0) = \begin{bmatrix} \delta(k;k_0) & 0 \\ 0 & \delta^{-1}(k;k_0) \end{bmatrix},$$
$$\delta(k;k_0) = \exp\left(\mathcal{C}_{(-\infty,k_0)}\tau(k)\right),$$

satisfies

$$\Delta^+(k;k_0) = \Delta^-(k;k_0)D(k), \quad k \in (-\infty,k_0),$$
$$\Delta(\infty;k_0) = I.$$

We multiply the solution of the RHP in Figure 4(b) by Δ^{-1} to remove the jump. To compute the solution to the new RHP we use

$$\begin{aligned} \Phi_1^+ &= \Phi_1^- J && \Leftrightarrow \\ \Phi_1^+\Delta_+^{-1} &= \Phi_1^- J\Delta_+^{-1} && \Leftrightarrow \\ \Phi_1^+\Delta_+^{-1} &= \Phi_1^-\Delta_-^{-1}\Delta_- J\Delta_+^{-1}. \end{aligned}$$

Indeed, we see that if $J = D$ there is no jump. Define $\Phi_2 = \Phi_1\Delta^{-1}$. See Figure 5 for a schematic overview of the new jumps. This deformation is not sufficient for a numerical solution as $\Delta(k;k_0)$ has a singularity at $k = k_0$. We must perform one last deformation in a neighborhood of $k = k_0$ to bound contours away from this singularity. We use a piecewise definition of a function Φ_3, see Figure 6(a), and compute the jumps, Figure 6(b). This is the final RHP. It is used, after contour truncation and scaling, to compute solutions of the NLS equations for arbitrarily large time. We discuss the scaling of the RHP in more detail in Section 7

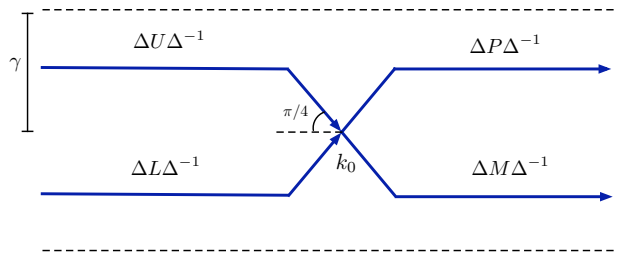

Figure 5: Removal of the jump on $(-\infty, k_0)$.

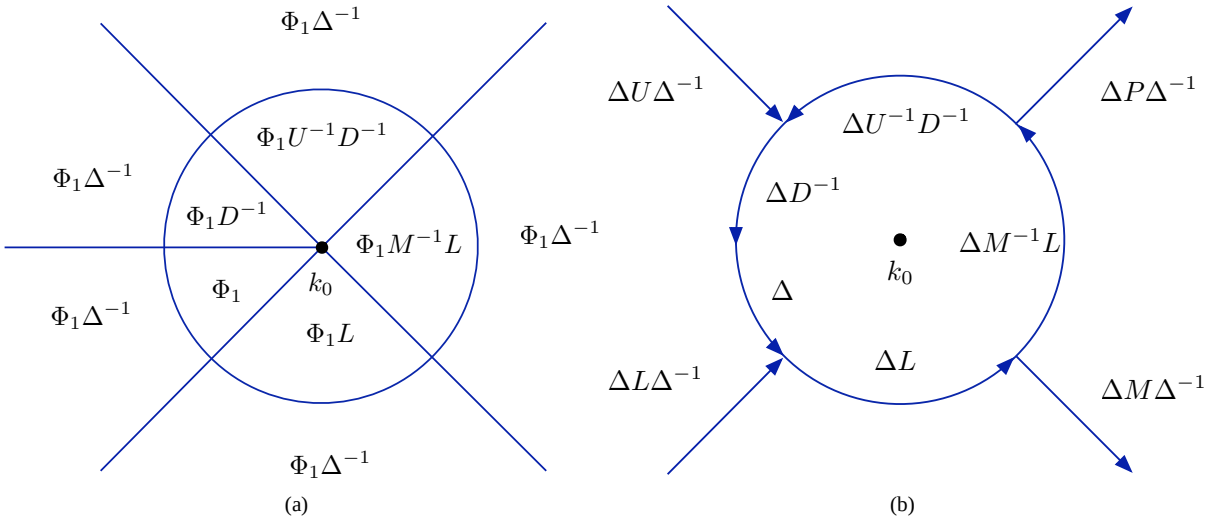

Figure 6: (a) The piecewise definition of Φ_3. (b) Jump contours and jump matrices for the RHP for Φ_3.

We use a combination of the deformation in Figure 4(b) for small time and the deformation in 6(b) to obtain an approximation to focusing or defocusing NLS when no solitons are present in the solution. Lastly, we deal with the addition of solitons for the case of focusing NLS. There are additional jumps of the form

$$\Phi^+(k) = \begin{cases} \Phi^-(k) \begin{bmatrix} 1 & 0 \\ -C_j e^{\theta(\kappa_j)}/(k-\kappa_j) & 1 \end{bmatrix}, & \text{if } k \in A_j^+, \\ \Phi^-(k) \begin{bmatrix} 1 & -\bar{C}_j e^{-\theta(\bar{\kappa}_j)}/(k-\bar{\kappa}_j) \\ 0 & 1 \end{bmatrix}, & \text{if } k \in A_j^-, \end{cases}.$$

We assume that $\mathrm{Re}(\kappa_j) > \gamma$.

For small x and t, $|e^{\theta(\kappa_j)}| = |e^{-\theta(\bar{\kappa}_j)}|$ is close to unity and the contours and jumps need to be added to one of the deformations discussed above. This will not be the case for all x and t. When $|C_j e^{\theta(\kappa_j)}| > 1$ we invert this factor through a deformation. Define the set $K_{x,t} = \{j : |C_j e^{\theta(\kappa_j)}| > 1\}$. Note that the x and t dependence enters through $\theta(\kappa_j)$. Next, define the functions

$$v(k) = \prod_{j \in K_{x,t}} \frac{k-\kappa_j}{k-\bar{\kappa}_j},$$

and

$$V(k) = \begin{bmatrix} v(k) & 0 \\ 0 & 1/v(k) \end{bmatrix}.$$

Define the piecewise-analytic matrix-valued function $\hat{\Phi}$:

$$\hat{\Phi}(k) = \Phi(k) \begin{cases} \begin{bmatrix} 1 & -(k-\kappa_j)/(C_j e^{\theta(\kappa_j)}) \\ C_j e^{\theta(\kappa_j)}/(k-\kappa_j) & \end{bmatrix} V(k), & \text{if } |k-\kappa_j| < \epsilon, \\ \begin{bmatrix} 0 & -\bar{C}_j e^{-\theta(\bar{\kappa}_j)}/(k-\bar{\kappa}_j) \\ (k-\bar{\kappa}_j)/(\bar{C}_j e^{-\theta(\bar{\kappa}_j)}) & 1 \end{bmatrix} V(k), & \text{if } |k-\bar{\kappa}_j| < \epsilon, \\ V(k) & \text{otherwise.} \end{cases}$$

Computing the jumps that $\hat{\Phi}$ satisfies we find, for $j \in K_{x,t}$,

$$\hat{\Phi}^+(k) = \hat{\Phi}^-(k) \begin{cases} V^{-1}(k) \begin{bmatrix} 1 & -(k-\kappa_j)/(C_j e^{\theta(\kappa_j)}) \\ 0 & 1 \end{bmatrix} V(k), & \text{if } k \in A_j^+, \\ V^{-1}(k) \begin{bmatrix} 1 & 0 \\ -(k-\bar{\kappa}_j)/(\bar{C}_j e^{-\theta(\bar{\kappa}_j)}) & 1 \end{bmatrix} V(k), & \text{if } k \in A_j^-. \end{cases}$$

This turns growth of the exponential to decay to the identity matrix. To simplify notation we define

$$T_{j,+}(k) = \begin{bmatrix} 1 & 0 \\ -C_j e^{\theta(\kappa_j)}/(k-\kappa_j) & 1 \end{bmatrix}, \tag{4.4}$$

$$T_{j,-}(k) = \begin{bmatrix} 1 & -\bar{C}_j e^{-\theta(\bar{\kappa}_j)}/(k-\bar{\kappa}_j) \\ 0 & 1 \end{bmatrix}, \tag{4.5}$$

$$S_{j,+}(k) = \begin{bmatrix} 1 & -(k-\kappa_j)/(C_j e^{\theta(\kappa_j)}) \\ 0 & 1 \end{bmatrix}, \tag{4.6}$$

$$S_{j,-}(k) = \begin{bmatrix} 1 & 0 \\ -(k-\bar{\kappa}_j)/(\bar{C}_j e^{-\theta(\bar{\kappa}_j)}) & 1 \end{bmatrix}. \tag{4.7}$$

In Figure 7 we present the full small-time and long-time RHPs. We use the notation $[J; \Sigma]$ to denote the RHP in Figure 7(b).

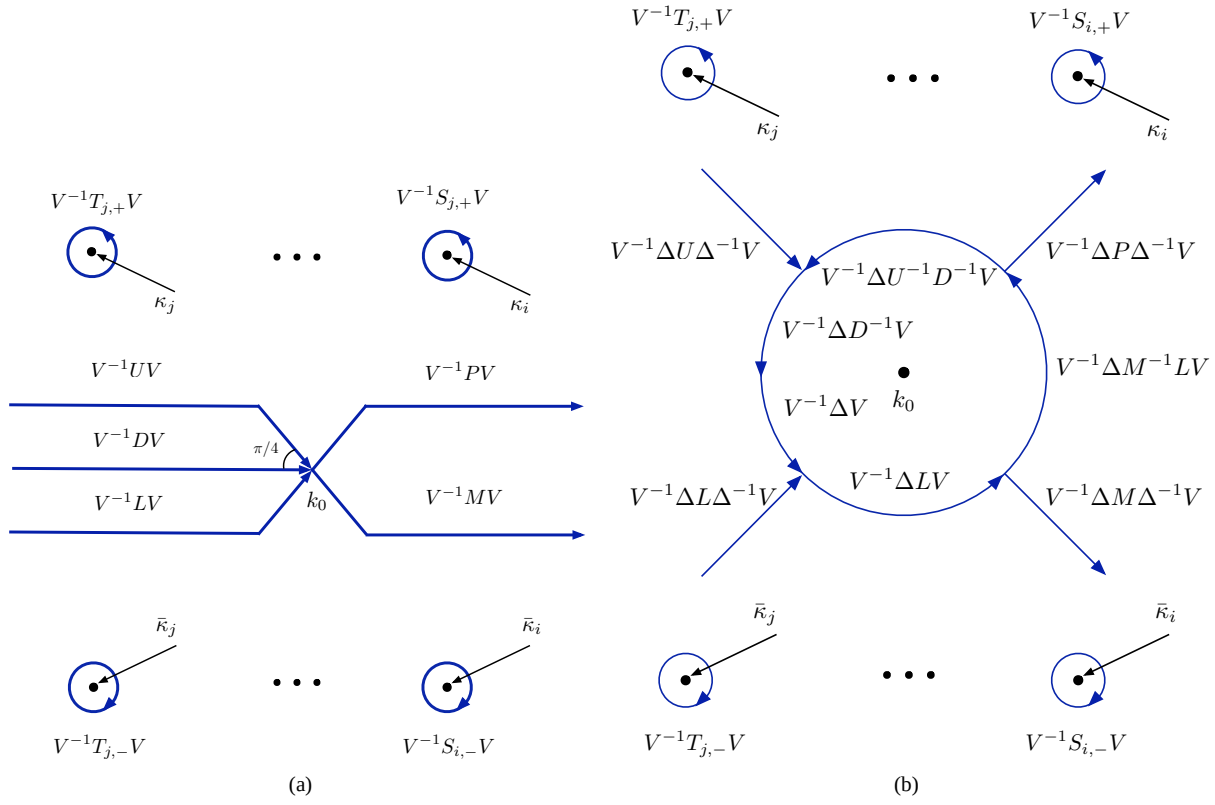

Figure 7: (a) The jump contours and jump matrices for the final deformation for small time. In this schematic $|C_j e^{\theta(\kappa_j)}| \leq 1$ and $|C_i e^{\theta(\kappa_i)}| > 1$. (b) The jump contours and jump matrices for the final deformation for large time. Again, in this schematic $|C_j e^{\theta(\kappa_j)}| \leq 1$ and $|C_i e^{\theta(\kappa_i)}| > 1$.

4.3 Numerical Results

In Figure 8 we plot the solution of the focusing NLS equation with q_0 given by (3.6) with $A = 1$ and $\mu = 0.1$. The solution is nearly reflectionless but Figure 8(d) shows the presence of dispersion. In Figure 10 we plot the initial condition $q_0(x) = 1.9\exp(-x^2 + ix)$. The solutions of the focusing and defocusing NLS equations with this initial condition are computed. See Figure 11 for focusing and Figure 12 for defocusing. We also note that when the initial condition is less localized the corresponding reflection coefficient is more oscillatory. This makes it more difficult to resolve the solution of the corresponding RHP. We restrict ourselves to localized initial data for this reason.

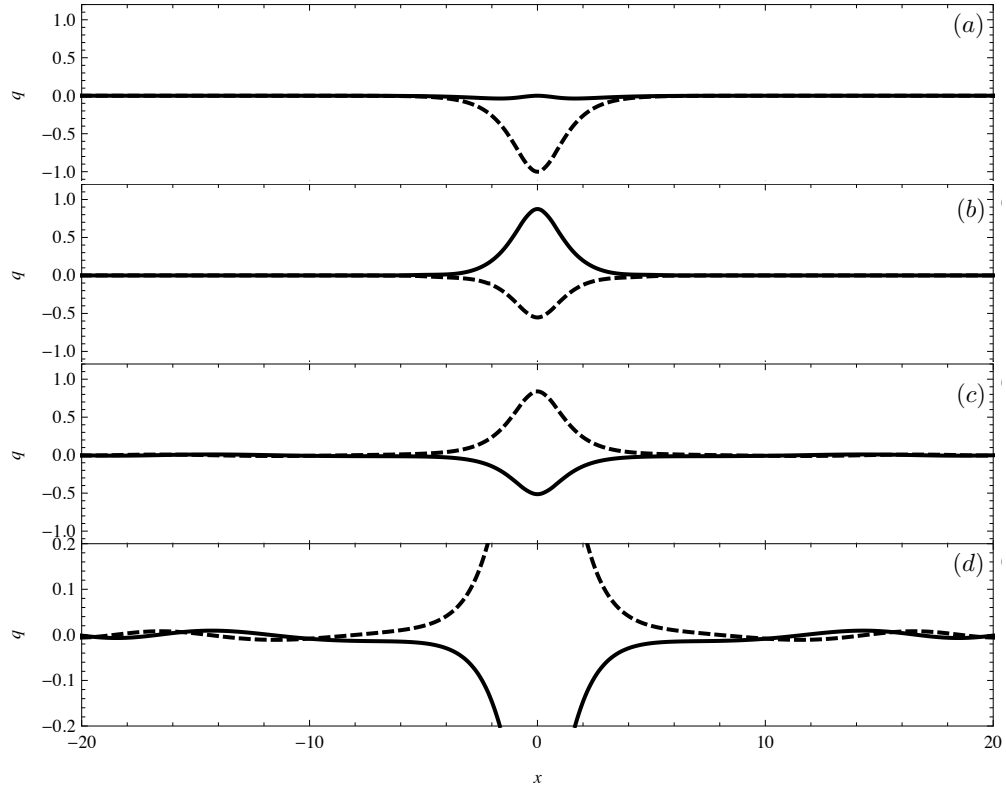

Figure 8: The solution of the focusing NLS equation with q_0 given by (3.6) with $A = 1$ and $\mu = .1$. (Solid: real part, Dashed: imaginary part) (a) $q(x, 0)$ (b) $q(x, 1)$ (c) $q(x, 10)$ (d) A scaled plot of $q(x, 10)$ showing the effects of dispersion.

We show numerical results that demonstrate spectral convergence. Let q_0 be given by (3.6) with $A = 1$ and $\mu = 0.1$ so that we can assume the reflection coefficient is computed to machine precision. Define $q(n, x, t)$ to be the approximate solution such that the number of collocation points per contour is proportional to n. In practice we set the number of collocation points to be n on shorter contours, like all contours in Figure 7(b). For larger contours, like the horizontal contours in Figure 7(a), we use $5n$ collocation points. To analyze the error we define

$$Q_m^n(x, t) = |q(n, x, t) - q(m, x, t)|. \tag{4.8}$$

Using this notation, see Figure 9 for a demonstration of spectral (Cauchy) convergence. Note that we choose x and t values to demonstrate spectral convergence in both the small time and large time regimes.

5 Extension to homogeneous Robin boundary conditions on the half line

The results thus far have been for the solution of the NLS equation posed on the whole line. We switch our attention to boundary-value problems on the half line, $x \geq 0$. Specifically, we extend the previous method to solve the following

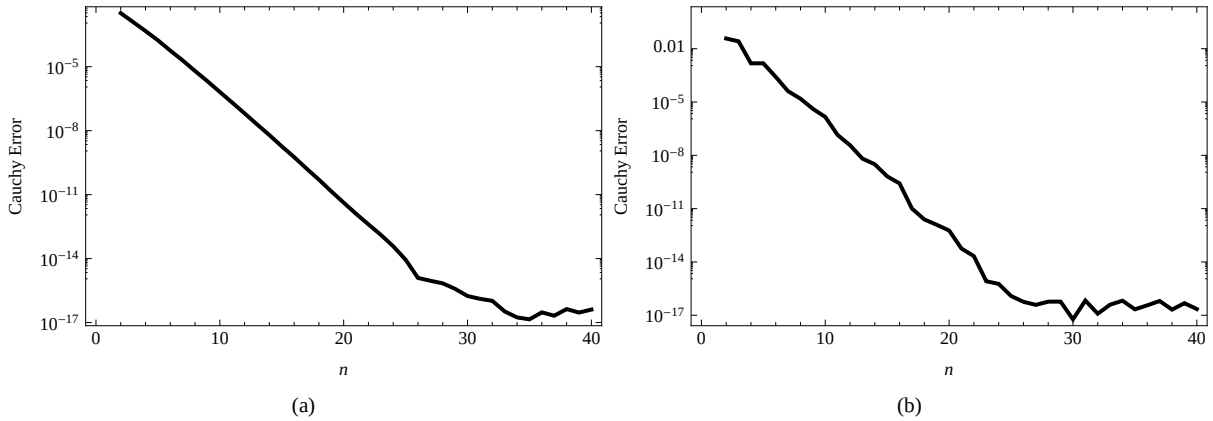

Figure 9: The convergence of the numerical approximations of the solution of the focusing NLS equation with q_0 given by (3.6) with $A = 1$ and $\mu = .1$. (a) $Q_n^{80}(2, 0.2)$ as n ranges from 2 to 40. (b) $Q_n^{80}(110, 110)$ as n ranges from 2 to 40.

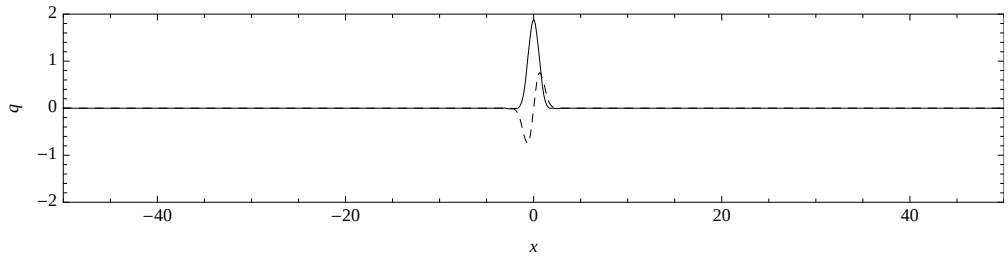

Figure 10: The initial condition $q_0(x) = 1.9e^{-x^2+ix}$. (Solid: real part, Dashed: imaginary part)

boundary-value problem:

$$\begin{aligned} iq_t + q_{xx} + 2\lambda|q|^2 q = 0, \;\; \lambda = \pm 1, \\ \alpha q(0,t) + q_x(0,t) = 0, \;\; \alpha \in \mathbb{R}, \\ q(x,0) = q_0(x) \in \mathcal{S}_\delta(\mathbb{R}^+), \delta > 0. \end{aligned} \tag{5.1}$$

Here $\mathcal{S}_\delta(\mathbb{R}^+)$ is the space of smooth functions f on $[0, \infty)$ such that

$$\limsup_{x\to\infty} e^{\delta x}|f(x)| < \infty.$$

If we take $\alpha = 0$ we obtain a Neumann problem and the limit $\alpha \to \infty$ effectively produces a Dirichlet problem. A method of images approach can be used to solve this problem. The approach of Biondini and Bui [3] takes the given initial condition on $[0, \infty)$ and produces an extension to $(-\infty, 0)$ using a Darboux transformation. For Neumann boundary conditions this results in an even extension and for Dirichlet boundary conditions the transformation produces an odd extension. Consider the system of ODEs

$$\begin{aligned} Y_1' &= Y_2, \\ Y_2' &= (4\lambda|q_0|^2 + \alpha^2)Y_1 - \lambda\bar{q}_0 Y_3 - q_0 Y_4, \\ Y_3' &= 2q_0' Y_1, \\ Y_4' &= 2\lambda\bar{q}_0' Y_1, \end{aligned} \tag{5.2}$$

with initial conditions

$$Y_1(0) = 1, \;\; Y_2(0) = -\alpha, \;\; Y_3(0) = 2q_0(0), \;\; Y_4(0) = 2\lambda\bar{q}_0(0),$$

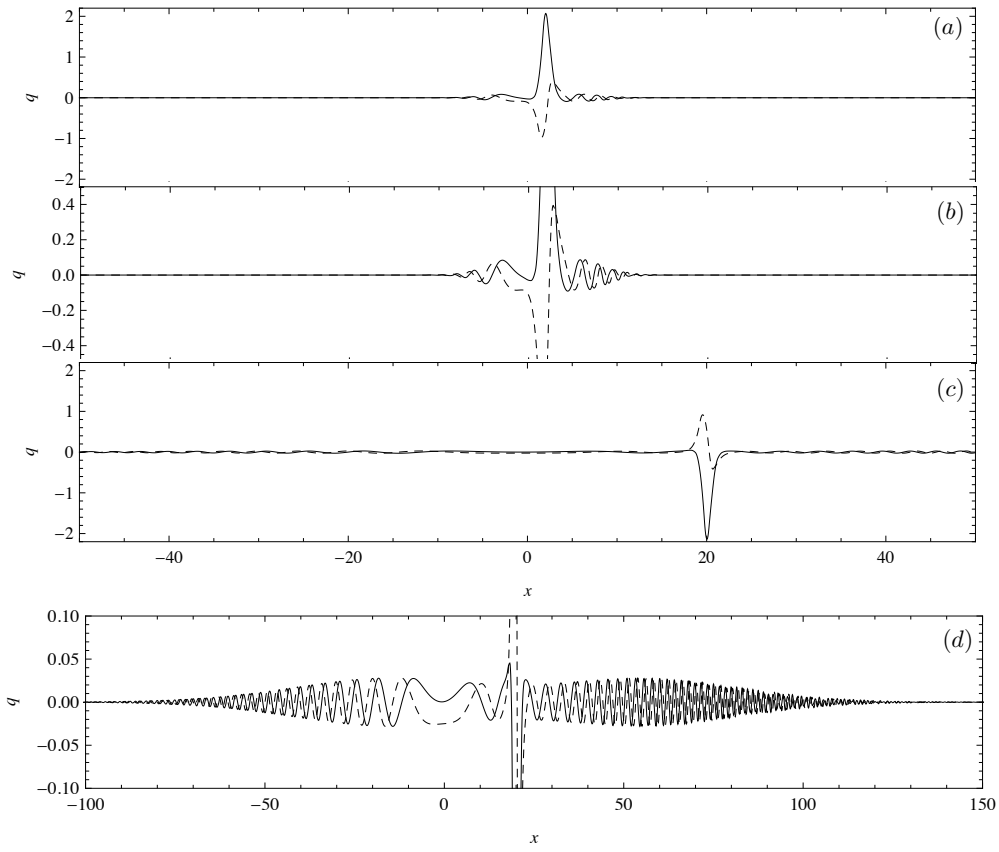

Figure 11: The solution of the focusing NLS equation with q_0 shown in Figure 10. (Solid: real part, Dashed: imaginary part) (a) $q(x,1)$ (b) A zoomed plot of $q(x,1)$ (c) $q(x,10)$ (d) A zoomed plot of $q(x,10)$, illustrating the dispersive effects in the solution.

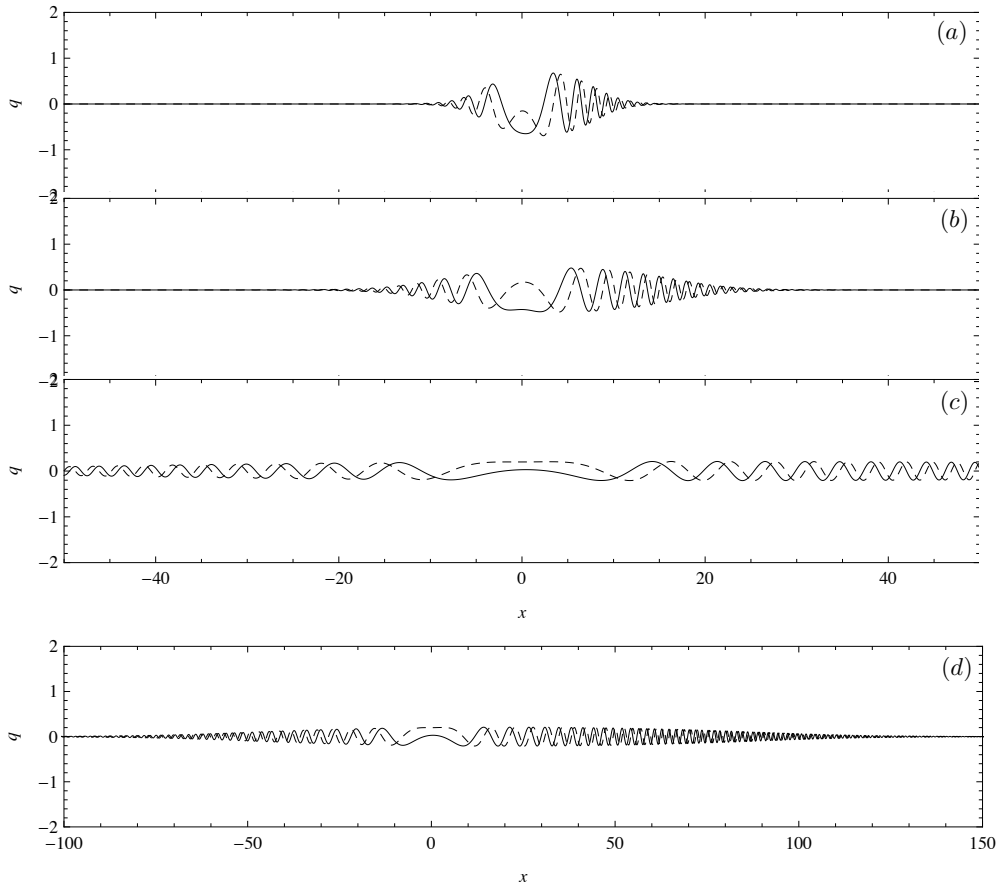

Figure 12: The solution of the defocusing NLS equation with q_0 shown in Figure 10. (Solid: real part, Dashed: imaginary part) (a) $q(x,1)$ (b) $q(x,2)$ (c) $q(x,10)$ (d) A scaled plot of $q(x,10)$ showing the dramatic effects of dispersion.

and the function

$$\tilde{q}(x) = \begin{cases} q_0(x), & \text{if } x \in [0,\infty), \\ -q_0(-x) + Y_3(x)/Y_1(x), & \text{if } x \in (-\infty, 0). \end{cases}$$

It was shown in [3] that the solution of the Cauchy problem for NLS equation on $\mathbb{R}$ with initial data $\tilde{q}$, restricted to $[0,\infty)$, is the unique solution of (5.1). To compute the extended initial data $\tilde{q}$ we first solve the system (5.2) numerically using a combination of Runge–Kutta 4 and 5. This is implemented in `NDSolve` in `Mathematica`. The IST for the extended potential can be used in the previous section's framework to numerically solve (5.1).

5.1 Numerical Results

In this section we show numerical results for a Robin problem and a Neumann problem. As noted above, we could treat the Dirichlet problem by using an odd extension of our initial condition.

- **Robin boundary conditions**

  Here we show results for the case of the focusing NLS equation ($\lambda = 1$) with $\alpha = -1$ and with initial condition $q_0(x) = 1.9\exp(-x^2 + x)$. Note that the initial condition satisfies the boundary condition at $t = 0$. In Figure 13(a), we give the extended initial condition $\tilde{q}$ and in Figure 13(b) we show the corresponding reflection coefficient. For this extended initial condition, we have four poles on the imaginary axis in the RHP which corresponds to two stationary solitons:

$$\begin{aligned} \kappa_1 &= 1.84725i, \quad C_1 = -14.4092i, \\ \kappa_2 &= 1.21265i, \quad C_2 = -8.17034i. \end{aligned}$$

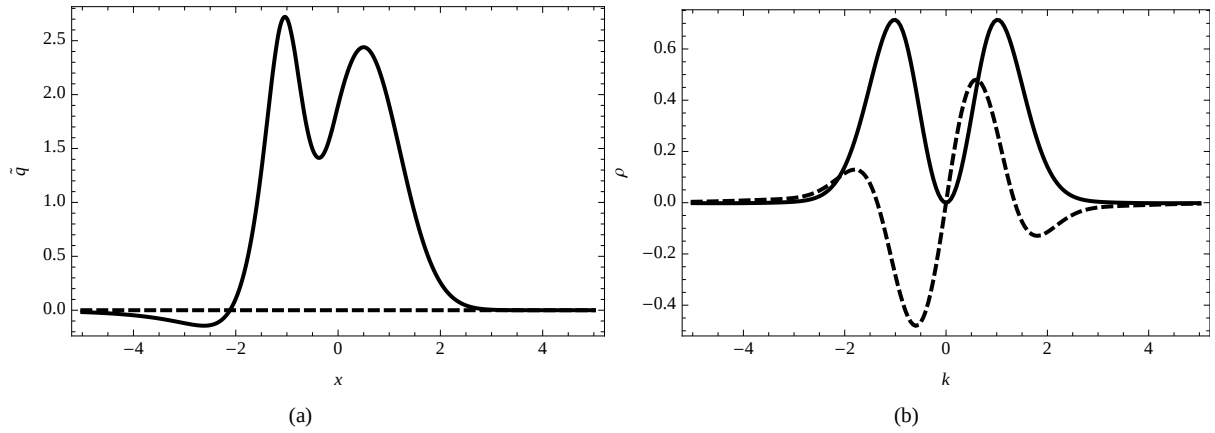

Figure 13: (a) The extended initial condition $\tilde{q}$ (Solid: real part, Dotted: imaginary part). (b) The reflection coefficient for the extended initial condition $\tilde{q}$. (Solid: real part, Dotted: imaginary part)

- **Neumann boundary conditions**

  To show the reflection of a soliton off the boundary at $x = 0$ we solve a Neumann problem ($\alpha = 0$) with initial condition $q_0(x) = 1/2x^2\exp(-.2x^2 - ix)$. The extension $\tilde{q}$ of the initial condition can be seen in Figure 15(a). In this case it is just the even extension. The scattering data consists of

$$\begin{aligned} \kappa_1 &= 0.497613 + 0.371208, \quad C_1 = 0.110159 + 5.35099i, \\ \kappa_2 &= -0.497613 + 0.371208, \quad C_2 = -0.231104 - 0.0357421i. \end{aligned}$$

  This shows that we have a pair of poles in the RHP to the right of the imaginary axis and two to left. This corresponds to one soliton moving to the left and one soliton moving to the right. The reflection coefficient is shown in Figure 15(b).

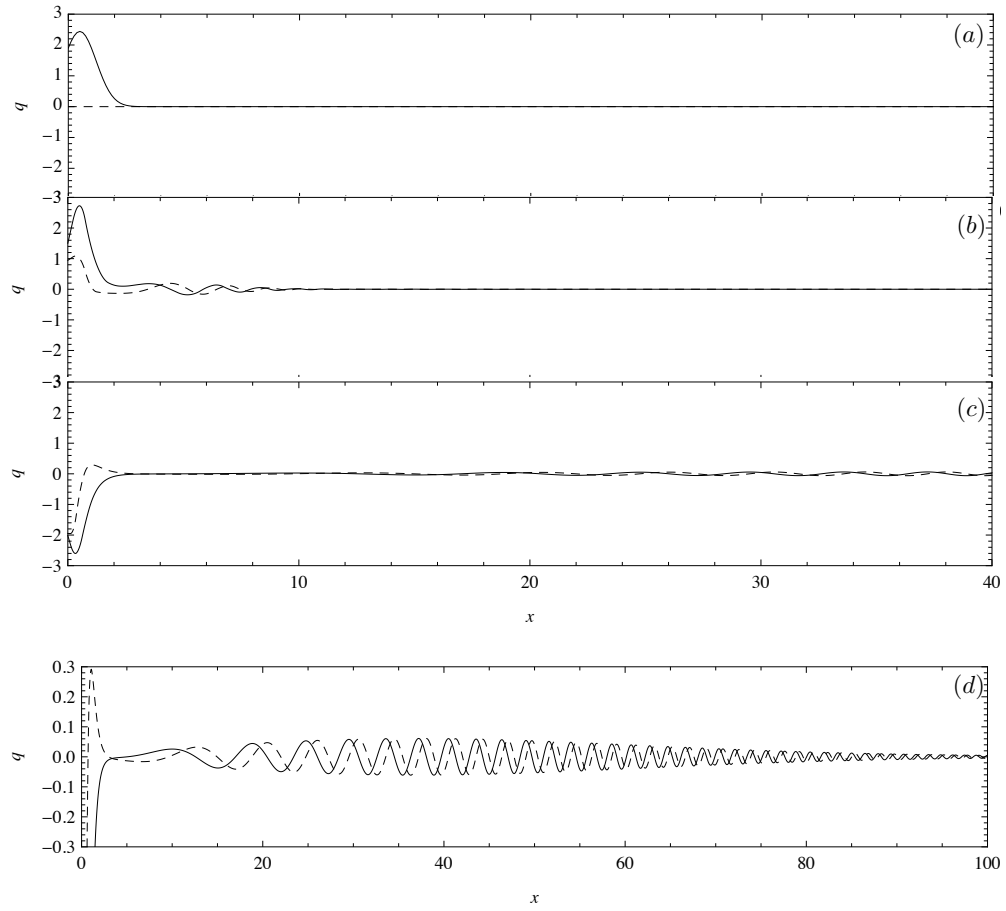

Figure 14: The solution of the focusing NLS equation with Robin boundary conditions ($\alpha = 1$) and with q_0 shown in Figure 13(a). (Solid: real part, Dashed: imaginary part) (a) $q(x, 0)$ (b) $q(x, 1)$ (c) $q(x, 10)$ (d) A scaled plot of $q(x, 10)$ showing the extent of the dispersive tail.

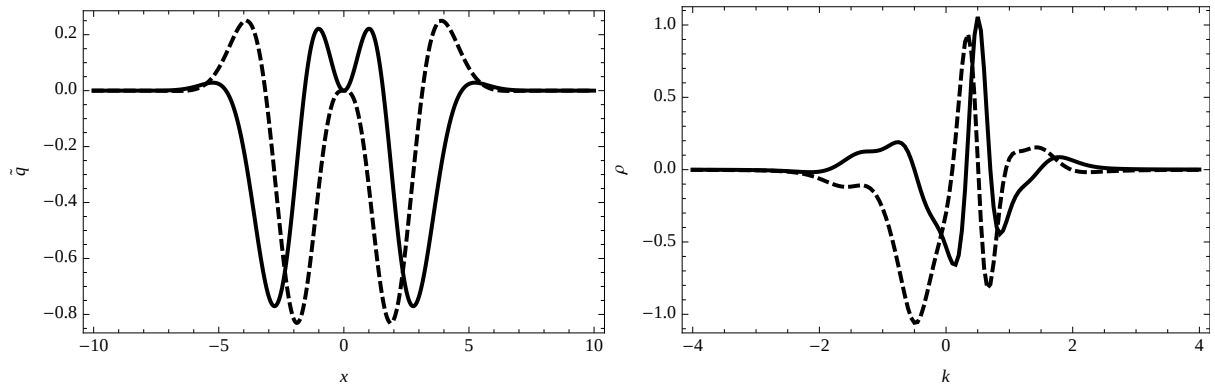

(a) (b)

Figure 15: (a) The extended initial condition $\tilde{q}$ (Solid: real part, Dotted: imaginary part). (b) The reflection coefficient for the extended initial condition $\tilde{q}$. (Solid: real part, Dotted: imaginary part)

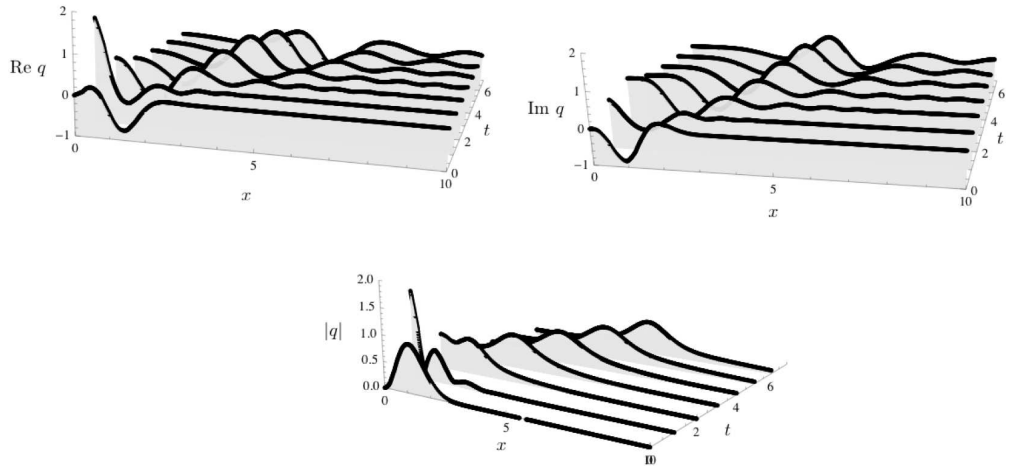

Figure 16: The solution of the focusing NLS equation Neumann boundary conditions and q_0 shown in Figure 15(a). The solution is obtained up to $t = 7$.

6 Singular solutions

As mentioned above the defocusing NLS equation does not have soliton solutions that decay at infinity. We can insert the contours $A_j^{\pm}$ (see (2.9)) into the RHP anyway. To get a solution of the defocusing NLS equation we need to make a generalization of (4.4) by adding λ. Define

$$
\begin{aligned}
T_{j,+}(k) &= \begin{bmatrix} 1 & 0 \\ -C_j e^{\theta(\kappa_j)}/(k-\kappa_j) & 1 \end{bmatrix}, \\
T_{j,-}(k) &= \begin{bmatrix} 1 & -\lambda \bar{C}_j e^{-\theta(\bar{\kappa}_j)}/(k-\bar{\kappa}_j) \\ 0 & 1 \end{bmatrix}, \\
S_{j,+}(k) &= \begin{bmatrix} 1 & -(k-\kappa_j)/(C_j e^{\theta(\kappa_j)}) \\ 0 & 1 \end{bmatrix}, \\
S_{j,-}(k) &= \begin{bmatrix} 1 & 0 \\ -\lambda(k-\bar{\kappa}_j)/(\bar{C}_j e^{-\theta(\bar{\kappa}_j)}) & 1 \end{bmatrix}.
\end{aligned}
$$

When $\lambda = 1$ (focusing) this definition agrees with (4.4).

When $\lambda = -1$ (defocusing) we investigate how these additional contours will manifest themselves in the solution. Consider

$$u_1(x,t) = 2\eta e^{-4it(\xi^2-\eta^2)-2ix\xi}\,\mathrm{sech}(2\eta(4t\xi + x - x_0)),$$

which is the one soliton solution of the focusing NLS equation [1]. A simple calculation shows that

$$u_2(x,t) = 2\eta e^{-4it(\xi^2-\eta^2)-2ix\xi}\mathrm{csch}(2\eta(4t\xi + x - x_0)),$$

is a solution of defocusing NLS. We are using the term solution loosely since this function has a pole when $2\eta 4t\xi + x - x_0 = 0$. We call this a singular solution or singular soliton. What we obtain when adding the above contours to the RHP associated with the defocusing NLS equation is a nonlinear combination of these singular solutions in the presence of dispersion, as in the focusing case where the soliton was nonsingular. See Figure 17 for plots of a solution obtained using the reflection coefficient in Figure 2 along with

$$\begin{aligned}\kappa_1 &= 2 + 2i, \quad C_1 = 1000,\\ \kappa_2 &= -2 + 2i, \quad C_2 = 1/1000.\end{aligned}$$

This corresponds to two of these singular solitons moving toward each other, until they bounce off each other (the poles never cross). They interact in the presence of dispersion. We choose large and small norming constants to have the solitons away from $x = 0$ when $t = 0$. It is not possible to obtain these types of solutions with traditional numerical methods. Not surprisingly, the relative accuracy of our numerical approximation breaks down near the poles. For points bounded away from the poles we still expect uniform convergence as discussed in the following section.

7 Asymptotic accuracy

In this section we use the theory of [24] to prove the accuracy of the numerical method for arbitrarily large time for $[J;\Sigma]$ in Figure 7(b). We assume the contours of the RHP are truncated according to Section 4. Define $\Sigma_1 = \bigcup_j (A_j^+ \cup A_j^-)$ and $\Sigma_2 = \Sigma \setminus \Sigma_1$. Define the restrictions of J:

$$\begin{aligned}J_1(k) &= J(k)|_{\Sigma_1},\\ J_2(k) &= J(k)|_{\Sigma_2}.\end{aligned}$$

We introduce some x and t independent domains Ω_1 and Ω_2:

$$\begin{aligned}\Sigma_1 &= \frac{\Omega_1}{\sqrt{t}} - \frac{x}{4t},\\ \Sigma_2 &= \Omega_2.\end{aligned}$$

We use the change of variables

$$k = \frac{z}{\sqrt{t}} - \frac{x}{4t}, \tag{7.1}$$

and the notation $\tilde{J}_1(z) = J_1(z/\sqrt{t} - x/(4t))$. Fix the trajectory in the (x,t) plane: $x = c4t$. We wish to apply the theory of [24]. To do this we need to modify our solution procedure. First, we numerically solve $[\tilde{J}_1, \Omega_1]$ with n collocation points to obtain a solution $\tilde{\Phi}_{1,n}$. The change of variables (7.1) is inverted, defining

$$\Phi_{1,n}(k) = \tilde{\Phi}_{1,n}\left(\sqrt{t}(k - k_0)\right).$$

Define $\tilde{J}_{2,n}(k) = \Phi_{1,n}(k)J_2(k)\Phi_{1,n}^{-1}(k)$. Then $[\tilde{J}_{2,n}, \Omega_2]$ is solved numerically with n collocation points (for simplicity) to obtain a function $\Phi_{2,n}$. Note that there is no change of variables to invert for this RHP. The function $\Phi_n = \Phi_{1,n}\Phi_{2,n}$ is an approximation of the solution to full RHP $[J;\Sigma]$.

Since the arc length of Σ_1 tends to zero for large t, the conditions we check are [24, Proposition 5.2]:

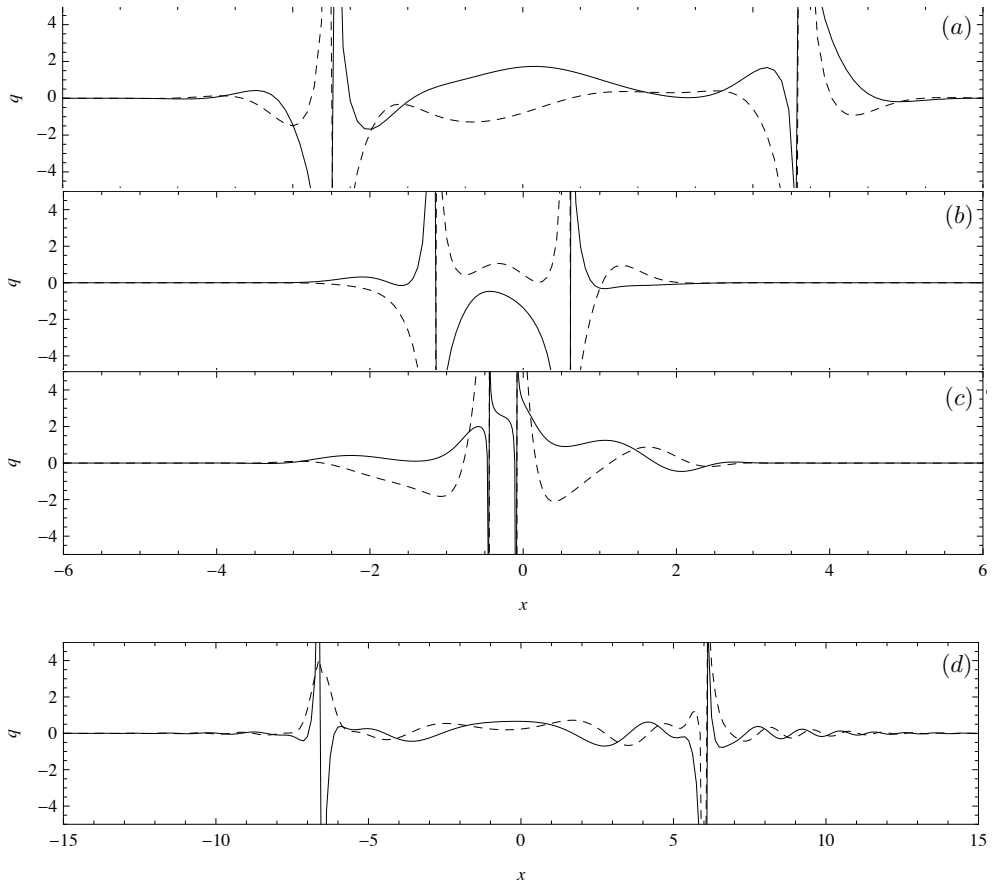

Figure 17: A singular solution of the defocusing NLS equation. Note that the vertical lines are asymptotes. (Solid: real part, Dashed: imaginary part) (a) $q(x,0)$ (b) $q(x,0.1)$ (c) $q(x,0.2)$, showing the interaction of the singular solutions. (d) $q(x,1)$, after the two poles have bounced off each other and a significant amount of dispersion is present.

- $\mathcal{C}[\tilde{J}_1;\Omega_1]^{-1}$ exists and is uniformly bounded in t,
- $\mathcal{C}[J_2;\Omega_2]^{-1}$ exists and is uniformly bounded in t, and
- all derivatives of $\tilde{J}_1(z)$ and $J_2(z)$, in the z variable, are uniformly bounded in t and z.

It is easy to see that all derivatives of $V^{-1}T_{j,\pm}V$ and $V^{-1}S_{j,\pm}V$ will be uniformly bounded. The transformation from $T_{j,\pm}$ to $S_{j,\pm}$ guarantees this.

The only possible singular behavior of $\tilde{J}_1$ will come from either the terms $\exp(\pm\theta(k))$ or from $\Delta(k;k_0)$. We proceed to show that under the chosen scaling, all derivatives of these two functions are bounded. From the definition of θ,

$$\theta(k) = 2i(c4tk + 2tk^2) = -4ic^2t + 4iz^2.$$

We see that all derivatives $\exp(\tilde{\theta}(z))$ are bounded as long as z is bounded.

Now we consider $\Delta(k;k_0)$ in a neighborhood of k_0. We need to bound derivatives of $\exp Y(k)$ where

$$Y(k) = \frac{1}{2\pi i}\int_{-\infty}^{k_0}\frac{f(s)}{s-k}ds, \quad f(s) = \log(1-\lambda\rho(s)\overline{\rho(s)}),$$

because it appears in Δ. We first note that $\exp(Y(k))$ is bounded for all k since $f(s)$ is real-valued. Now, since the Cauchy integral is invariant under a conformal change of variables that leaves infinity fixed, we have

$$\begin{aligned}\tilde{Y}(z) &= \frac{1}{2\pi i}\int_{-\infty}^{0}\frac{\tilde{f}(s)}{s-z}ds,\\ \tilde{f}(s) &= f(s/\sqrt{t} - x/(4t)), \quad \tilde{Y}(z) = Y(z/\sqrt{t} - x/(4t)).\end{aligned}$$

From [17] (see also [24]) we have

$$\begin{aligned}\tilde{Y}^{(j)}(z) &= \frac{1}{2\pi i}\left(\int_{-\infty}^{0}\frac{\tilde{f}^{(j)}(s)}{s-z}ds - \sum_{i=1}^{j}\frac{\tilde{f}^{(j-i)}(0)}{(-z)^{i+1}}\right),\\ \tilde{f}^{(j)}(0) &= f^{(j)}\left(-\frac{x}{4t}\right)t^{-j/2}.\end{aligned}$$

From the assumption that ρ is analytic and decays in a strip containing the real line we see that all derivatives of $\tilde{Y}$ are uniformly bounded in t.

The analysis in [24] requires that the singular integral operators on Ω_i have uniformly bounded inverses as t becomes large. This follows from the asymptotic analysis of the RHP [10, 9]. While we made the restriction $x = 4ct$ above, the bounds on derivatives can be taken to be independent of c. Define W^i to be the solution of the SIE on Ω_i, see (2.11) and W_n^i to be its approximation with n collocation points per contour. We arrive at the following theorem.

Theorem 7.1. *For sufficiently large t and every $\epsilon > 0$ there exists $N > 0$ such that for $n > N$*

$$\|W_n^i - W^i\|_{L^2(\Omega_i)} < \epsilon, i = 1, 2.$$

Remark 7.1. *This theorem relies heavily on Assumption 4.1. If Assumption 4.1 fails to be true the numerical method may not converge.*

Since the arc length of the contours is bounded we have uniform $L^1(\Gamma)$ convergence and (4.2) demonstrates that $q(x,t)$ is approximated uniformly.

7.1 Numerical Results

To demonstrate asymptotic accuracy we use the notation in (4.8) and fix n and m. We let x and t become large along a specific trajectory. For our purposes we use $x = 4t$. Note that along this trajectory q is on the order of $1/\sqrt{t}$ [31] (see also [10, 9, 8]). This allows us to estimate the relative error. See Figure 18 for a demonstration of the accuracy of the method for large x and t. We see that the relative error is bounded and small using relatively few collocation points.

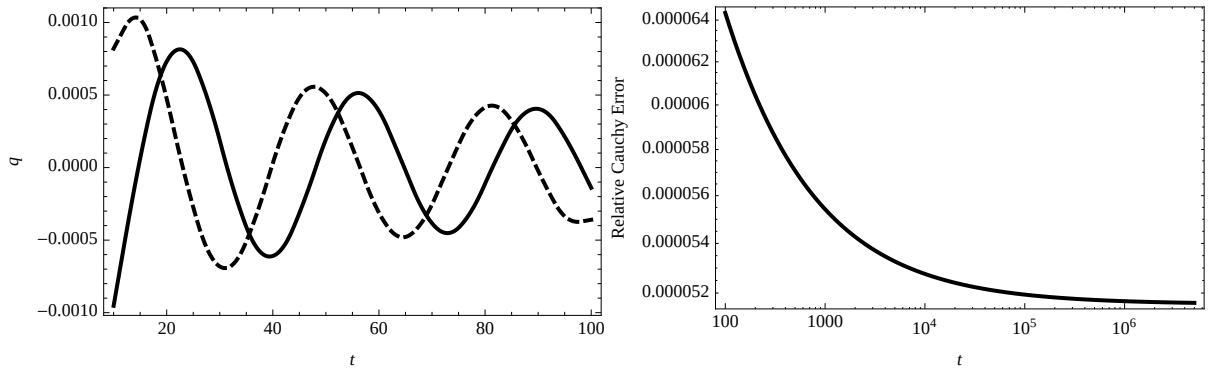

(a) (b)

Figure 18: Asymptotic computations of solutions of the focusing NLS equation with q_0 given by (3.6) with $A = 1$ and $\mu = .1$. (Solid: real part, Dashed: imaginary part) (a) $q(8, 4t, t)$. (b) $Q_8^{16}(4t, t) \cdot t^{1/2}$ for large values of t.

8 Conclusions

We are able to successfully compute the full IST on the whole line for smooth initial data with sufficiently fast decay and compute singular solutions if we use special spectral data. All spectral data can be obtained with spectral accuracy. Furthermore, numerical extensions of data on the half line can be used to solve homogeneous Dirichlet, Neumann and Robin boundary-value problems on the half line. After deforming the contours of the RHP in the spirit of Deift and Zhou and the method of nonlinear steepest descent, we obtain a method that is accurate for arbitrarily large values of x and t. More precisely, the computational cost required to compute the solution accurate to within a given tolerance can be shown to be independent of x and t.

9 Acknowledgments

We thank Bernard Deconinck for many useful conversations and Gino Biondini for suggesting the numerical solution of boundary-value problems. We acknowledge the National Science Foundation for its generous support through grant NSF-DMS-1008001 (TT). Any opinions, findings, and conclusions or recommendations expressed in this material are those of the authors and do not necessarily reflect the views of the funding sources.

References

[1] M. J. Ablowitz. *Nonlinear dispersive waves*. Cambridge Texts in Applied Mathematics. Cambridge University Press, New York, 2011. Asymptotic analysis and solitons.

[2] M. J. Ablowitz and P. A. Clarkson. *Solitons, Nonlinear Evolution Equations and Inverse Scattering*. Cambridge University Press, 1991.

[3] G. Biondini and A. Bui. On the nonlinear schrdinger equation on the half line with homogeneous robin boundary conditions. *Studies in Applied Mathematics*, pages no–no, 2012.

[4] G. Boffetta and A. R. Osborne. Computation of the direct scattering transform for the nonlinear Schrödinger equation. *J. Comp. Phys*, 102:252–264, 1995.

[5] C.W. Curtis and B. Deconinck. On the convergence of Hill's method. *Math. Comp.*, 79(269):169–187, 2010.

[6] B. Deconinck and J. N. Kutz. Computing spectra of linear operators using the Floquet–Fourier–Hill method. *Journal of Comp. Phys.*, 291(1):296–321, 2007.

[7] P. Deift and X. Zhou. A steepest descent method for oscillatory Riemann–Hilbert problems. *Bulletin AMS*, 26:119–124, 1992.

[8] P. Deift and X. Zhou. Long-time asymptotics for integrable systems. Higher order theory. *Comm. Math. Phys.*, 165(1):175–191, 1994.

[9] P. Deift and X. Zhou. *Long-time behavior of the non-focusing nonlinear Schrödinger equation—a case study*, volume 5 of *Lectures in Mathematical Sciences*. University of Tokyo, 1994.

[10] P. Deift and X. Zhou. Long-time asymptotics for solutions of the NLS equation with initial data in a weighted Sobolev space. *Comm. Pure Appl. Math.*, 56:1029–1077, 2003.

[11] T. Grava and C. Klein. Numerical solution of the small dispersion limit of Korteweg–de Vries and Whitham equations. *Comm. Pure Appl. Math.*, 60:1623–1664, 2007.

[12] E. P. Gross. Strucure of a quantized vortex in boson systems. *Il Neuvo Cimento*, 20:454–477, 1961.

[13] O. H. Hald. Numerical solution of the Gel'fand–Levitan equation. *Linear Algebra Appl.*, 28:99–111, 1979.

[14] M. A. Johnson and K. Zumbrun. Convergence of Hill's method for non-self adjoint operators. *SIAM J. Numer. Anal.*, 50(1):64–78, 2012.

[15] C. Klein. Fourth order time-stepping for low dispersion Korteweg–de Vries and nonlinear Schrödinger equations. *Elect. Trans. Numer. Anal.*, 29:116–135, 2008.

[16] S. V. Manakov. On the theory of two-dimensional stationalry self-focusing of electromagnetic waves. *Soviet Physics JETP*, 48(2):248–253, 1974.

[17] S. G. Mikhlin and S. Prössdorf. *Singular Integral Operators*. Springer, 1980.

[18] N. I. Muskhelishvili. *Singular Integral Equations*. Groningen: Noordoff, (based on the second Russian edition published in 1946) edition, 1953.

[19] F. W. J. Olver, D. W. Lozier, R. F. Boisvert, and C. W. Clark. *NIST Handbook of Mathematical Functions*. Cambridge University Press, 2010.

[20] S. Olver. RHPackage. http://www.maths.usyd.edu.au/u/olver/projects/RHPackage.html.

[21] S. Olver. Fast, numerically stable computation of oscillatory integrals with stationary points. *BIT*, 50(1):149–171, 2010.

[22] S. Olver. Computing the Hilbert transform and its inverse. *Math. Comp.*, 80:1745–1767, 2011.

[23] S. Olver. A general framework for solving Riemann–Hilbert problems numerically. *Numer. Math.*, 2011. To appear.

[24] S. Olver and T. Trogdon. Nonlinear steepest descent and the numerical solution of Riemann–Hilbert problems. `arXiv:1205.5604 [math.NA]`, 2012.

[25] A. Osborne. *Nonlinear Ocean Waves and the Inverse Scattering Transform*. Academic Press, 2010.

[26] L. P. Pitaevskii. Vortex lines in a imperfect Bose gas. *Sov. Phys., JETP*, 13:451–454, 1961.

[27] A. Tovbis, S. Venakides, and X. Zhou. On semiclassical (zero dispersion limit) solution of the focusing nonlinear Schrödinger equation. *Comm. Pure Appl. Math.*, 57:877–985, 2004.

[28] T. Trogdon, S. Olver, and B. Deconinck. Numerical inverse scattering for the Korteweg–de Vries and modified Korteweg–de Vries equations. *Physica D*, 241(11):1003–1025, 2012.

[29] V. E. Zakharov. Stability of periodic waves of finite amplitude on the surface of a deep fluid. *J Appl. Mech. Tech. Phys.*, 9(2):190–194, 1968.

[30] V. E. Zakharov and S. V Manakov. On the complete integrability of a nonlinear Schrödinger equation. *J. Theor. Math. Phys.*, 19(3):551–559, 1974.

[31] V. E. Zakharov and S. V Manakov. Asymptotic behavior of non-linear wave systems integrated by the inverse scattering method. *Soviet Physics JETP*, 44(1):106–112, 1976.

[32] V. E. Zakharov and A. B. Shabat. Exact theory of two-dimensional self-focusing and one-dimensional solf-modulation of waves in nonlinear media. *Soviet Physics JETP*, 34(1):62–69, 1972.